Journal of Materials and Environmental Sciences
ISSN : 2028-2508
CODEN : JMESCN

J. Mater. Environ. Sci., 2018, Volume 9, Issue 3, Page 1058-1074

https://doi.org/10.26872/jmes.2017.9.3.118

http://www.jmaterenvironsci.com

Camphor as an effective corrosion inhibitor for carbon steel in 1M HCl solution: electrochemical and quantum chemical investigation

H. Bourazmi[1], M. Tabyaoui[1], L. EL Hattabi[1], Y. El Aoufir[1,2], E.E. Ebenso[3], A. Ansari[4]

[1] *Laboratory of Nanotechnology, Materials & Environment, Faculty of Sciences, Mohammed V University, Rabat, Morocco*
[2] *Laboratory of Separation Processes, Faculty of Sciences, University Ibn Tofail, Kenitra, Morocco*
[3] *Department of Chemistry and Material Science Innovation & Modelling (MaSIM) Research Focus Area, Faculty of Agriculture, Science and Technology, North-West University, Private Bag X2046, Mmabatho 2735, South Africa*
[4] *Université My Ismail, Faculté Polydisciplinaire, BP 512, 52003, Errachidia, Morocco*

Received 14 May 2017,
Revised 21 Jan 2018,
Accepted 23 Jan 2018

Keywords
- ✓ Corrosion,
- ✓ Carbon steel,
- ✓ Inhibition,
- ✓ Camphor,
- ✓ Adsorption,
- ✓ Impedance,
- ✓ Polarization curves.

M. Tabyaoui
hamidtabyaoui@yahoo.fr

Abstract

The inhibition of corrosion of carbon steel by camphor in hydrochloric acid (1M HCl) was tested, using electrochemical techniques (impedance spectroscopy (EIS) and potentiodynamic polarization (PDP) and quantum chemical calculations (QCC). Impedance measurements showed that the double-layer capacitance decreased and charge transfer resistance increased with the rise of the inhibitor concentration, which explains the increase in inhibition efficiency. Potentiodynamic polarization techniques reveal that the presence of the inhibitor does not change the mechanism of hydrogen evolution. The effect of temperature on the corrosion behavior of carbon steel in 1 M HCl with and without addition of camphor was studied in the temperature range between 303 and 333 K. Phenomenon of physical adsorption is proposed from the activation parameter obtained. Thermodynamic parameters show that the adsorption process is spontaneous. Quantum chemical calculations using DFT were used to calculate some electronic properties of the molecule in order to ascertain the correlation between the inhibitive effect and the molecular structure of the camphor molecule.

1. Introduction

The use of inhibitors is one of the most practical methods for protection of corrosion, especially in acidic media [1-4]. The hydrochloric acid is also an important acid with many uses in some industries [5-7]. The adsorption of organic inhibitors depends mainly on the electronic and structural properties of the inhibitor molecule such as functional groups, aromaticity, electron density on donor atoms and π orbital character of donating electrons [8–14]. The corrosion inhibitors organic, having heteroatom's in their aromatic or long carbon chain [15], those that are non-toxic or low-toxic to both human and environment [16-37].

The strict environmental legislations and increasing ecological awareness among scientists have led to the development of "green" alternatives to mitigate corrosion. Recently, natural compounds such as herb plants were employed as inhibitors in order to develop new cleaning chemicals for green environment [38-39]. Plants are rich sources of naturally synthesized chemical compounds (organic acids, glucosinolates, alkaloids, polyphenols, and tannins) and most are known to have inhibitive action [38, 40]. Most of the natural products are non-toxic and biodegradable. Various parts of the plants, leaves, fruits, seeds, and flowers [41-46] were extracted and used as corrosion inhibitors. Several literature reviews on the suitability of natural products such as essential oils and its major components as corrosion inhibitors of steel in chlorhydric acid were recently published [47-51].

This work contributes to develop the green corrosion inhibitors and investigates the inhibiting effect of camphor against corrosion of carbon steel in a 1M HCl medium. Camphor (Figure 1) is a major component of salvia officinalis oil. It is a white or transparent solid with a strong aromatic odor and a naturally occurring component of some volatile essential oils [52]. It is a terpenoid with the chemical formula $C_{10}H_{16}O$. It is found in the wood of the camphor laurel (Cinnamomum Camphora), a large evergreen tree found in Asia (particularly in Sumatra, Indonesia and Borneo) and also of the unrelated Kaptur tree, a tall timber tree from the same region.

It is also present in the mint family, which contain up to 20% camphor. Camphor is used for its scent, as an ingredient in cooking (mainly in India), as an embalming fluid, for medicinal purposes, and in religious ceremonies. Theoretical calculations have been used recently to explain the mechanism of corrosion inhibition. The geometry of the inhibitor molecule in its ground state, the nature of its molecular orbitals HOMO (Highest Occupied Molecular Orbital) and LUMO (Lowest Unoccupied Molecular Orbital) are directly involved in the corrosion inhibition activity. In continuation of our previous study, the present work is devoted to the investigation of the corrosion inhibition by adsorption of camphor on carbon steel in chlorhydric acid by potentiodynamic polarization (PDP), electrochemical impedance spectroscopy (EIS) and quantum chemical calculations in detail. The molecular structure of this compound is shown in Figure 1.

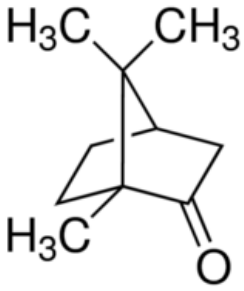

Figure 1: Molecular structure of camphor

2. Experimental details

2.1. Materials

In this study we have used carbon steel (C35) (Euronorm: C35E carbon steel and US specification: SAE 1035) with a chemical composition (in wt%) of 0.370 % C, 0.230 % Si, 0.680 % Mn, 0.016 % S, 0.077 % Cr, 0.011% Ti, 0.059 % Ni, 0.009 % Co, 0.160 % Cu and the remainder iron (Fe).

2.2. Solutions

The aggressive solutions of 1 M HCl were prepared by dilution of analytical grade 37% HCl with distilled water. The concentration of camphor was in the range between 1.31 mM and 7.88 mM.

2.3. Electrochemical impedance spectroscopy

The electrochemical measurements were carried out using a Volta lab (Tacussel- Radiometer PGZ 100) potentiostate and controlled by a Tacussel corrosion analysis software model (Voltamaster 4) under static conditions. The corrosion cell used had three electrodes. The reference electrode was a saturated calomel electrode (SCE). A platinum electrode was used as auxiliary electrode with surface area of 1 cm2. The working electrode was made of carbon steel. All potentials given in this study were referred to this reference electrode. The working electrode was immersed in a test solution for 30 minutes to a establish the steady state open circuit potential (Eocp). After measuring the Eocp, the electrochemical measurements were performed. All electrochemical tests have been performed in aerated solutions at 303 K. The EIS experiments were conducted in the frequency range of 100 kHz to 10 mHz at open circuit potential, with 10 points per decade, at the rest potential, after 30 min of acid immersion, by applying 10 mV peak-to-peak ac voltage. Nyquist plots were made from these experiments. The inhibition efficiency of the inhibitor was calculated from the charge transfer resistance values using the following equation:

$$\eta_{EIS}\% = \frac{R^{\circ}_{ct} - R^{i}_{ct}}{R^{\circ}_{ct}} \times 100 \qquad (1)$$

Where, R°_{ct} and R^{i}_{ct} are the charge transfer resistance in absence and in presence of the inhibitor, respectively.

2.4. Potentiodynamic polarization

The electrochemical behavior of carbon steel in inhibited and uninhibited solution was studied by recording anodic and cathodic potentiodynamic polarization curves. Measurements were performed in the 1.0 M HCl solution containing different concentrations of the tested inhibitor by changing the electrode potential automatically from -800 to -300 mV versus corrosion potential at a scan rate of 1mV.s^{-1}. The linear Tafel segments of the anodic and cathodic curves were extrapolated to corrosion potential to obtain the corrosion current densities (I_{corr}). From the polarization curves obtained, the corrosion current (I_{corr}) was calculated using the equation:

$$I = I_{corr}\left[\exp\left(\frac{2.3\,\Delta E}{\beta_a}\right) - \exp\left(\frac{2.3\,\Delta E}{\beta_c}\right)\right] \qquad (2)$$

The inhibition efficiency was evaluated from the measured Icorr values using the following relationship:

$$\eta_{\text{Tafel}}\% = \frac{I^{\circ}_{\text{corr}} - I^{i}_{\text{corr}}}{I^{i}_{\text{corr}}} \times 100 \qquad (3)$$

Where, I°_{corr} and I^{i}_{corr} are the corrosion current density in absence and presence of the inhibitor, respectively.

2.5. Quantum chemical calculations

Complete geometrical optimizations of the investigated molecule are performed using density functional theory (DFT) with the Becke's three parameter exchange functional along with the Lee–Yang–Parr nonlocal correlation functional (B3LYP) with 6-31G* basis set as implemented in the Gaussian 09 program package[53]. Theoretical parameters such as the energies of the highest occupied and lowest unoccupied molecular orbital (EHOMO and ELUMO), energy gap (ΔE) and dipole moment (μ) absolute electronegativity (χ), global hardness (γ) and softness (σ), and fraction of electrons transferred (ΔN) were calculated.

2.6. Molecular Dynamics Simulations details

MD simulations were carried out using Materials Studio 8.0 (from Biovia-Accelrys Inc.). The box consisted of a 6 layers of iron atoms cleaved along the (110) plane. A supercell of (10 × 10) simulation box was created, and a liquid phase (500 water molecules) and vacuum layer of 20 nm height was fabricated. During the simulation, all 6 layers of iron atoms were fixed. One camphor molecule was optimized and included in the simulation box using the amorphous cell module. The simulation was carried out using For cite module with a time step of 1 fs and simulation time of 500 ps performed at 298 K, NVT ensemble, using COMPASS force field [54-56].

3. Results and discussion

3.1. Electrochemical experiments

3.1.1. OCP vs. time measurements

The potentiostatic curves E=f(t) are illustrated in Figure 2 without and with various concentrations of camphor ranging between 1.38 and 7.88 mM. According to this Figure, the initial value of E_{corr} was -0.456 (mV/SCE) in blank the solution, and it becomes almost constant around -0.584(mV/SCE) after 600s. The addition of inhibitors in aggressive solution, cause a slight displacement of E_{corr} during the immersion. The variation of corrosion potential values in the presence of the inhibitor compared with the blank solution can be explained by the adsorption of the inhibitor compounds on the metal surface. The potentiodynamic polarization and impedance values have been measured after 30 minute of immersion.

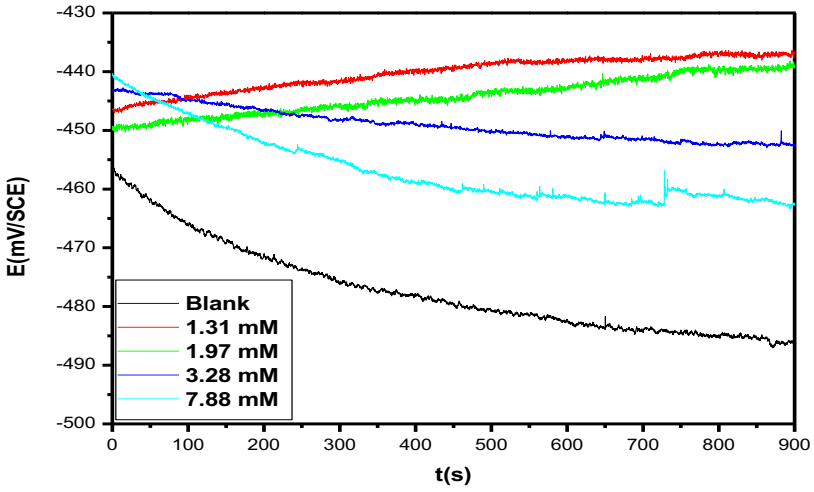

Figure 2: Variation of the open circuit potential versus time of the carbon steel in 1 M HCl solutions and containing different concentrations of camphor at 303K

3.1.2. *Polarization measurements*

The electrochemical measurements were carried out to understand the kinetic process of the anodic and cathodic reactions. The work electrode was maintained at its free potential during 30 min. After a period of immersion, the polarization curves have been also illustrated for 10 min. Figure 3 shows that the corrosion potential is

varied between -800 mV and -300 mV with a scan rate of 1 mV/s. The polarization curves of carbon steel in chlorhydric acid solution (1M HCl) containing different concentration of camphor at 303K are presented in Figure 3. Table 1 shows the electrochemical corrosion parameters such as corrosion potential (E_{corr}), cathodic and anodic Tafel slope (β_a,β_c), corrosion current density (I_{corr}), inhibition efficiency η_{Tafel} (%) and degree of surface coverage (θ) were derived from the potentiodynamic polarization curves. It can be seen from Figure 3 that the existence of inhibitor molecule in the corrosive medium increases anodic and cathodic over potentials, and decreases corrosion current (I_{corr}). These changes increase with increasing inhibitor concentration. This behavior supports the adsorption of inhibitor onto metal surface and causes a barrier effect for mass and charge transfer for anodic and cathodic reactions. However Table 1 shows markedly that the addition of camphor decreases the corrosion current density and hence the inhibition efficiency η_{Tafel} (%) increases with the inhibitor concentration to reach its maximum value, 72.10 %, at 7.88 mM. This behavior explains its ability to inhibit the corrosion of carbon steel (C35) in chlorhydrique acid solution .The slight variation of the cathodic Tafel slope (β_c) upon addition of camphor indicates that the cathodic corrosion mechanism of carbon steel does not change, but the small changes in the anodic Tafel slope (β_a) values are probably due to the adsorption of chloride ions or inhibitor on the metal surface (C35). According to literature if the displacement in E_{corr} is more than ±85mV relative to the corrosion potential of the blank solution, the inhibitor can be considered as a cathodic or anodic type, if the change in E_{corr} is less than ±85 mV, the corrosion inhibitor may be regarded as a mixed type [57,58]. In our study, the presence of this compound in acidic media causes a slight displacement of corrosion potential compared to the blank solution, shift in E_{corr} values is in the range of 21-37 mV, which indicates that the inhibitor tested act as mixed-type inhibitor [52-59].

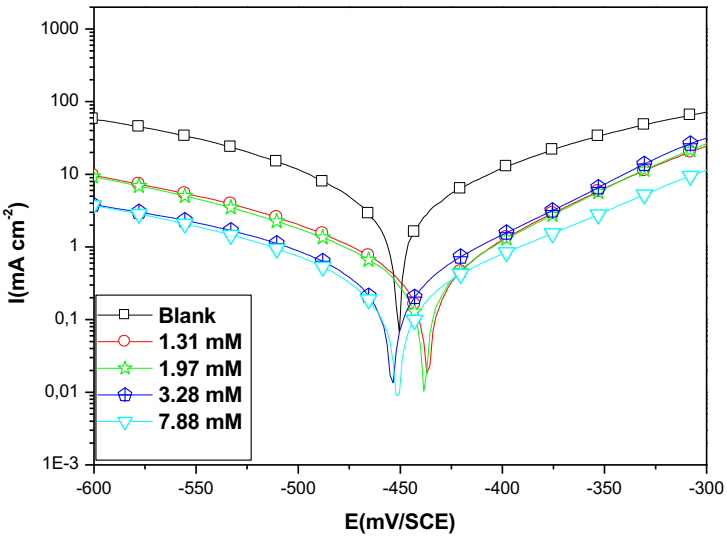

Figure 3: Anodic and cathodic polarization curves for the corrosion of carbon steel in 1 M HCl in the absence and presence of different concentrations of camphor at 303K

Table1: Electrochemical parameters calculated by using the potentiodynamic polarization technique for the corrosion of carbon steel in 1 M HCl in the absence and presence of different concentrations of camphor at 303K

Medium	Conc mM	$-E_{corr}$ (mV/SCE)	I_{corr} (µA/cm^2)	β_a (mV)	$-\beta_c$ (mV)	η_{Tafel} %	Θ
1 M HCl	-	-452	507	100	122	-	-
Camphor	1.31	437	281.0	42.3	67.8	44.58	0.4458
	1.97	438	213.1	42.9	59	57.97	0.5797
	3.28	453	166.6	42.6	61	67.14	0.6714
	7.88	450	128.8	55	60	74.60	0.7460

3.1.3. Electrochemical impedance spectroscopy (EIS)

Measurements of the corrosion inhibition of carbon steel in the 1M HCl medium in absence and presence of various concentrations in Camphor were studied with the EIS method at 303 K, after an immersion time of 30 minutes. The results obtained are presented as Nyquist plots (see Figure 4). The impedance spectra are represented as one single capacitive loop, which is attributed to the charge transfer at the carbon steel /solution interfaces. However, the shape of the capacitive loops suggests that the charge transfer process controls the corrosion of carbon steel [63,64]. On the other hand, the diameter of the capacitive loop increases with the rise of the inhibitor concentration compared to the behaviour observed in the absence of the inhibitor. We have noted that, the depressed semi-circle in Nyquist diagram is not perfect. This has been attributed to the frequency dispersion as well as to the heterogeneity due to surface roughness, impurities or dislocations [65], fractal structures [66].The inhibitor is adsorbed on activity centers which lead to the formation of porous layers [67].

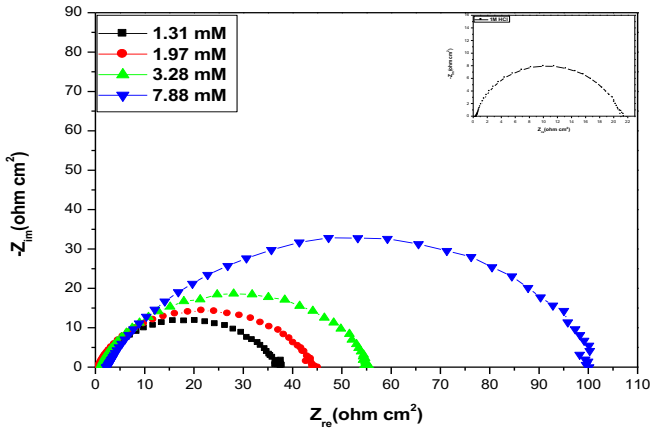

Figure 4: Nyquist plots for carbon steel in 1M HCl solution without and with different concentration of camphor at 303K

Figure 5: Equivalent circuit used to fit the EIS data

The electrochemical parameters, comprise the solution resistance R_s, the charge transfer resistance R_{ct}, the constant phase element (Q), empirical exponent (n) and the time constant (τ), obtained from fitting the recorded EIS data are listed in Table 2. The capacitance is replaced with a constant phase element (CPE). The electrochemical equivalent circuit used to model the metal/acidic solution interface is shown in Figure 5. The impedance (Z) of CPE is given by the expression [68]:

$$Z_{CPE} = Q^{-1}(j\omega)^{-n} \qquad (4)$$

Where Q is proportionality coefficient (in Ω^{-1} s^n cm^{-2}), ω is the angular frequency, j is the imaginary number and n is the CPE exponent which gives details about the degree of the surface inhomogeneity resulting. The double layer capacitance values (C_{dl}) are calculated using the following equation [68-70]:

$$C_{dl} = (QR_{ct}^{1-n})^{\frac{1}{n}} \qquad (5)$$

$$\tau = C_{dl}R_{ct} \qquad (6)$$

It is very clear after the in Table 2 that the camphor inhibits the corrosion of carbon steel in 1 M HCl solution, at all concentrations used in this study, which confirms the increase in the charge transfer resistance (R_{ct}) as the concentration rises and consequently the protection efficiency increases. Also, the value of the proportional factor Q of CPE decreases with increasing of the inhibitor concentration. The change of R_{ct} and the Q values can be related to the gradual replacement of the water molecules and the other ions originally adsorbed on the surface by the camphor molecule and consequently to a decrease in the number of active sites necessary for the corrosion

reaction [71]. The factor values (n) increases with increasing of the camphor concentration (see Table 2). This data can be explained by the reduction of the surface inhomogeneity due to the adsorption of the inhibitor on the most active sites [72].

Table 2: Electrochemical parameters for carbon steel electrode corresponding to the EIS data in 1.0 M HCl solution in the absence and the presence of various concentrations of camphor

Medium	Conc. (mM)	R_s (Ω cm^2)	R_{ct} (Ω cm^2)	$10^4 A$ (Ω^{-1} s^n cm^{-2})	n	C_{dl} (μF cm^{-2})	τ (s)	η_Z (%)
1M HCl	-	0.5558	20	4.715	0.8619	223.33	0,0044	-
camphor	1.31	0.9669	35.46	3.973	0.8796	221.68	0,0078	43.59
	1.97	0.6882	42.27	3.295	0.8927	197.13	0,0083	52.68
	3.28	1.0150	53.91	2.698	0.8929	162.43	0,0087	62.90
	7.88	2.2880	99.00	1.550	0.8949	94.90	0,0093	79.79

However, the addition of the inhibitor in free solution decreases merely the double layer capacitance (C_{dl}) (Table 2), while the time constant (τ) value increases from 0.0044 s in the blank solution to 0.0093 s in 7.88 mM camphor. This decrease in C_{dl} with an increase in inhibitor concentrations may be attributed to the formation of a protective layer on the electrode surface [73]. This trend is in accordance with the Helmholtz model, given by the following equation [74]:

$$C_{dl} = \frac{\varepsilon\varepsilon_\circ}{d} \qquad (7)$$

Where d is the thickness of the protective layer, ε is the dielectric constant of the protective layer and ε_0 is the permittivity of free space(8.854×10^{-14} F cm^{-1}).This data signify that the presence of the inhibitor in the chlorhydric acidic solution decrease charge and discharge rates to the metal-solution interface. The double layer formed between the corrosion solution and the charged metal surface is considered as an electrical capacitor. These results show that the inhibitor tested has a protective effect in each concentration and the protection efficiency η_Z(%) increases with increasing of the concentration; the maximum inhibition efficiency was achieved at 7.88 mM.

3.1.4. Effect of temperature

The temperature has an effect on the corrosion inhibition. This problem is very complex, because many changes exist occur on the surface of the metal such as desorption of inhibitor. The effect of temperature on the inhibition performance of camphor for carbon steel in 1M HCl solution in the absence and presence of 7.88mM the inhibitor at temperature ranging from 303 to 333 K was obtained by potentiodynamic polarization measurements (Figures 6; (a) and (b)). The results are given in Table 3.

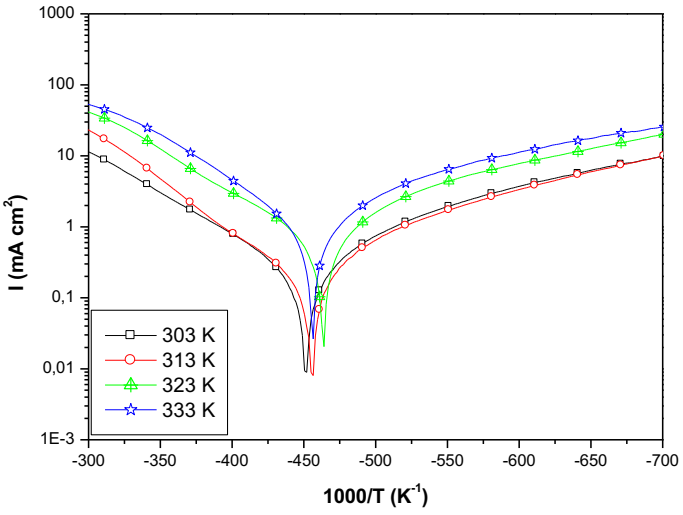

Figure 6: Potentiodynamic polarization curves of carbon steel in 1 M HCl in the absence and presence of the optimum concentration of camphor at different temperatures

Table 3: Electrochemical parameters and the corresponding inhibition efficiencies at various temperature studied of carbon steel in 1M HCl in absence and presence 7.88 mM of camphor

Inhibitor	Temperature (K)	E_{corr} (mV/SCE)	i_{corr} ($\mu A\ cm^{-2}$)	η(%)
Blank	303	-452	507	-
	313	-454	860	-
	323	-443	1840	-
	333	-450	2800	-
Camphor	303	-450	129	74.60
	313	-455	291	66.16
	323	-461	639	65.27
	333	-455	1138	59.35

The dependence of the corrosion rate on the temperature can be expressed by the Arrhenius equation [75]: The rise of the temperature, leads to a decrease of inhibition efficiency. This behavior can be interpreted that the inhibition efficiency depends of the temperature, confirming that camphor acts as an efficient inhibitor for the carbon steel in 1M HCl in the studied temperature range. The results can be explained by the decrease of the adsorption process at the highest temperature, and one can suggest a physical adsorption mode. Table 3 shows that the corrosion current density (I_{corr}) increases more rapidly with the increasing temperature both in uninhibited and inhibited solutions.

$$I_{corr} = k \exp\left(\frac{-Ea}{RT}\right) \qquad (8)$$

Where E_a is the apparent activation corrosion energy, R is the universal gas constant and k is the Arrhenius pre-exponential constant Arrhenius plots for the corrosion density of carbon steel in the case of camphor are given in Figure 7. The values of corrosion apparent activation energy (E_a) for carbon steel in 1 M HCl with the absence and presence of camphor were determined from the slope of Ln (I_{corr}) versus 1/T plots and shown in table 4.

According to the literature [76], the higher value of E_a was considered as physisorption that occurred in the first stage. There are two possibilities for these active centers with different E_a on the metal surface: (1) the activation energy in the presence of the inhibitors is lower than that of pure acidic medium, namely $E_a(inh) < E_a(HCl)$, which suggests a smaller number of more active sites remain uncovered in the corrosion process; (2) the activation energy in the presence of inhibitor is higher than that of the pure acidic medium, $E_a(inh) > E_a(HCl)$, which represents the inhibitor adsorbed on the most active adsorption sites (having the lowest energy) and the corrosion takes place chiefly on the active sites (having higher energy).

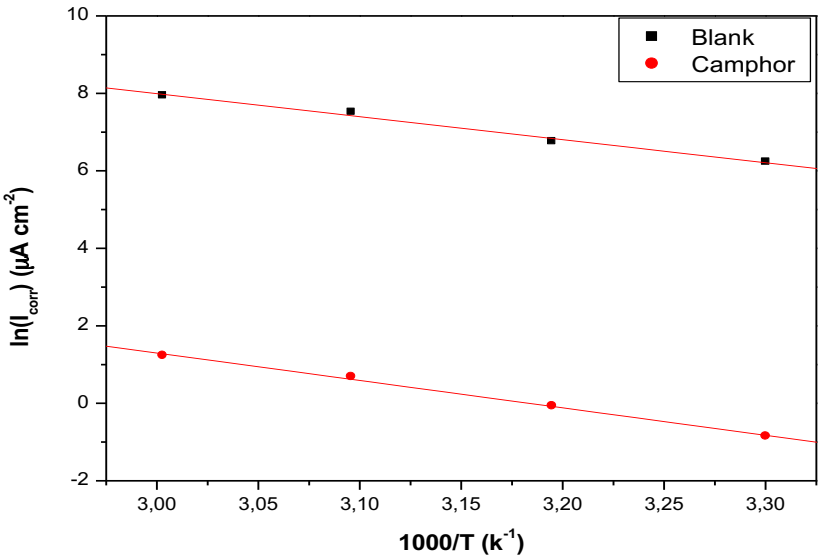

Figure 7: Arrhenius plots of the carbon steel in 1M HCl with and without 8.33mM of Camphor

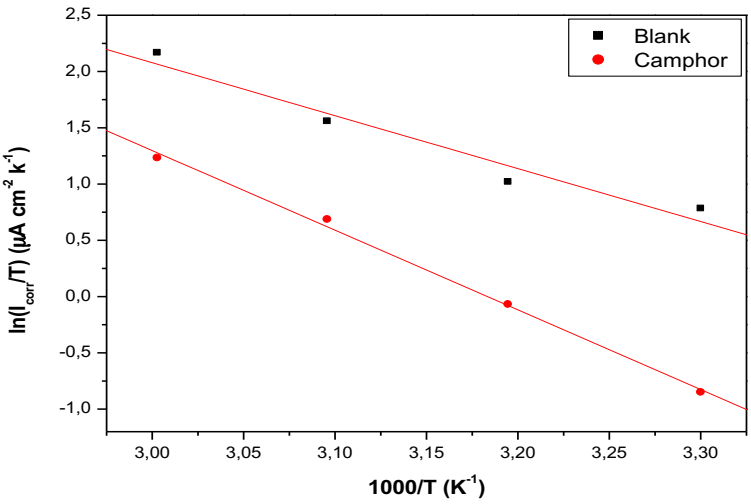

Figure 8: Transition Arrhenius plots of the carbon steel in 1M HCl with and without 7.88 mM of camphor

Table 4: The values of activation parameters E_a, ΔH and ΔS for carbon steel in1M HCl in the absence and presence of mM of camphor

Inhibitor	E_a ($KJ.mol^{-1}$)	ΔH ($KJ.mol^{-1}$)	ΔS ($J.mol^{-1}.K^{-1}$)	E_a- ΔH
Blank	41.72	39.12	-62.896	2.6
Camphor	61.478	58.838	-10.475	2.6

The data in Table 4 specifically indicate that the value of E_a in the presence of camphor is larger than that in the absence of camphor. Thus, it is clear that the adsorption of camphor on the carbon steel surface blocks the active sites from acid solution and consequently increases the apparent activation energy. Then, it can be suggested that the camphor adsorb by physisorption on the metallic surface. Activation parameters like enthalpy (ΔH) and entropy (ΔS) for the dissolution of carbon steel in 1 M HCl in the absence and presence of camphor were calculated from the transition state equation (Eq. (9)) [77]:

$$\ln\left(\frac{I_{corr}}{T}\right) = \frac{R}{Nh}\exp\left(-\frac{\Delta H}{RT}\right)\exp\left(\frac{\Delta S}{R}\right) \qquad (9)$$

Where I_{corr} is the corrosion rate, A is the pre-exponential factor, h is Planck's constant, N is the Avogadro number, R is the universal gas constant, ΔH_a is the enthalpy of activation and ΔS_a is the entropy of activation. Figure 8 showing the Arrhenius plots of Ln (I_{corr}/T) versus 1/T give straight lines with slope (-ΔH/R) and intercept (Ln R/Nh + ΔS/R) from which ΔH and ΔS values were calculated. The activation parameters are given in Table 5.The positive sign of the enthalpies ΔH_a reflects the endothermic nature of the steel dissolution process. ΔS (HCl) < ΔS (inh), suggests an increase in disorder.

3.2. Adsorption isotherm

The mechanism of the interaction between inhibitor and the electrode surface can be explained using adsorption isotherms. The fractional surface coverage θ for different concentrations of camphor in 1 M HCl solution can easily be determined using the flowing formula:

$$\theta = \frac{I_{corr} - I_{corr(i)}}{I_{corr}} \times 100 \qquad (10)$$

As it is known that the adsorption of an organic molecule onto metal-solution interface can be presented as a substitution adsorption process between the organic molecules in the aqueous solution $Org_{(sol)}$ and the water molecules on the metallic surface $H_2O_{(ads)}$:

$$Org_{(sol)} + n\,H_2O_{(ads)} \leftrightarrow Org_{(ads)} + n\,H_2O_{(sol)}$$

$Org_{(sol)}$ and $Org_{(ads)}$ are the organic molecules in the aqueous solution and adsorbed on the metallic surface, respectively, $H_2O_{(ads)}$ is the water molecules on the metallic surface, n is the size ratio representing the number of water molecules replaced by one molecule of organic adsorbate.

Several models of the adsorption isotherms process of camphor in the carbon steel surface such as: Langmuir, Temkin and Frumkin, were obtained according to the following equations:

$$\text{Langmuir:} \quad \frac{C_{inh}}{\theta} = \frac{1}{K_{ads}} + C_{inh} \qquad (11)$$

$$\text{Frumkin:} \quad \frac{\theta}{1-\theta}\exp(-2a\theta) = bC_{inh} \qquad (12)$$

$$\text{Temkin:} \quad \exp(-2a\theta) = bC_{inh} \qquad (13)$$

$$\text{Freundlich:} \quad Log(\theta) = Log(K) + nLog(C) \qquad (14)$$

Where θ is the surface coverage of the metal surface, K_{ads} the adsorption-desorption equilibrium constant, C_{inh} the inhibitor concentration and a is the lateral interaction term describing the molecular interactions in the adsorption layer and the heterogeneity of the surface, n is generally positive constant and not an integer constant. The fractional coverage values θ as a function of the inhibitor concentration can be obtained from the potentiodynamic polarization.

To determine which adsorption is the best fitting isotherm the surface coverage; the respective plots were obtained in Figures (9 – 12). These curves represent the adsorption isotherms that are characterized by, in a first part, a sharp rising, followed by another part, a gradual rising (less significant than in the first part), indicating formation of an adsorbed molecular layer on the steel surface. By far, the best fit was obtained with the Langmuir isotherm (strong correlation R^2 =0.99745.). The plots of C_{inh}/θ vs. C_{inh} yield a straight line (Figure 9).

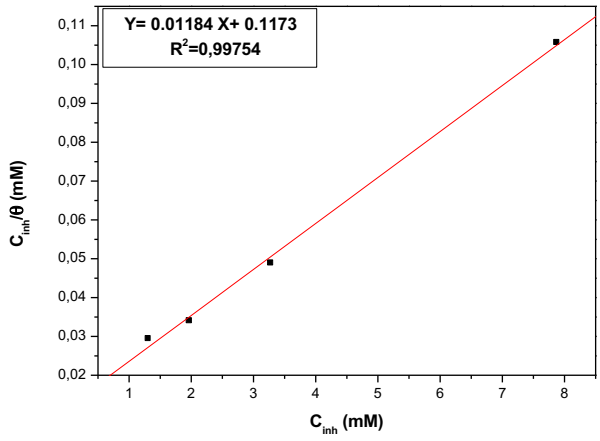

Figure 9: Langmuir adsorption plots obtained for carbon steel in 1 M HCl containing different concentrations of camphor

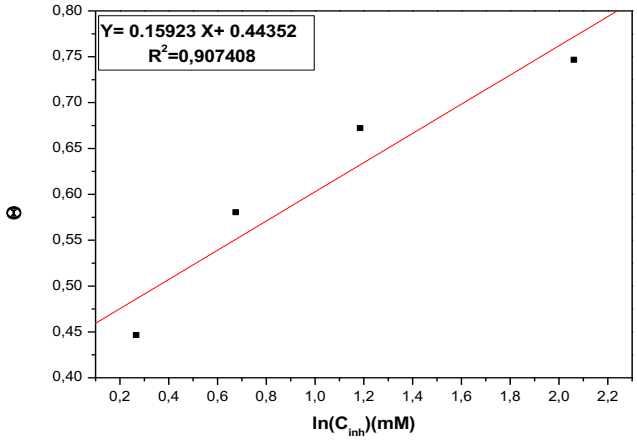

Figure 10: Temkin adsorption plots obtained for carbon steel in 1 M HCl containing different concentrations of camphor

This confirms that the inhibitor obeys Langmuir adsorption isotherm at 1M HCl medium. K_{ads} is related to the standard free energy of adsorption (ΔG°_{ads}), according to [78]:

$$K_{ads} = \frac{1}{C_{H_2O}} \exp\left(\frac{\Delta G^{\circ}_{ads}}{RT}\right) \qquad (15)$$

Where R is the universal gas constant, T the thermodynamic temperature and C_{H2O} the concentration of water in the solution which is 55500 mM.

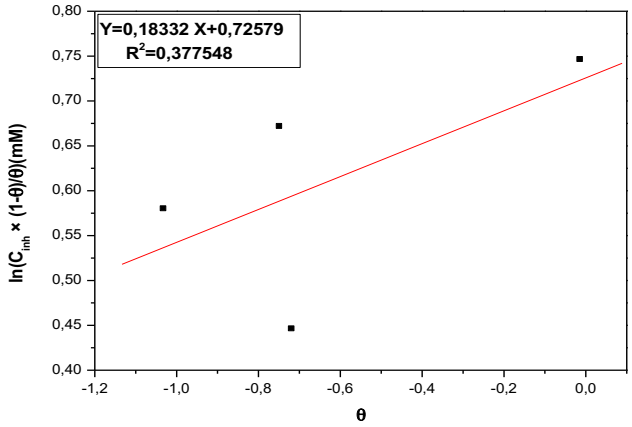

Figure 11: Frumkin adsorption plots obtained for carbon steel in 1 M HCl containing different concentrations of camphor

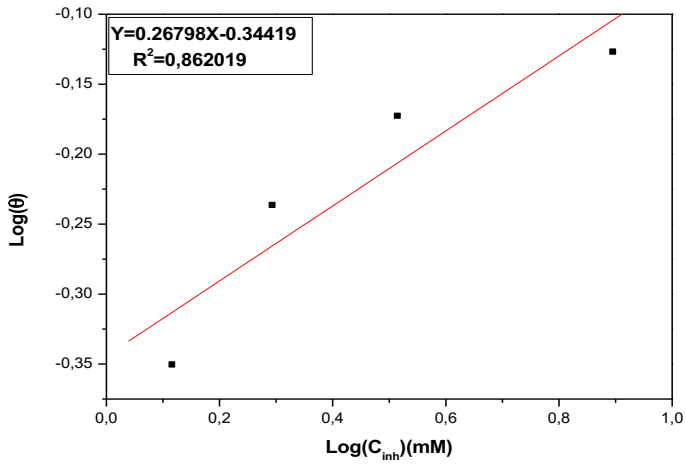

Figure 12: Freundlich adsorption plots obtained for carbon steel in 1 M HCl containing different concentrations of camphor

Table 5: Values of parameters the adsorption of camphor on the mild steel in 1 M HCl

Inhibitor	K_{ads} (mM^{-1})	$-\Delta G^{\circ}_{ads}$ ($KJ.mol^{-1}$)	R^2
Camphor	8.52514919	22.80	0.99754

Generally, energy values of ΔG°_{ads} around -20 KJ mol^{-1} are associated with an electrostatic interaction between charged inhibitor molecules and charged metal surface, called physisorption. Those of -40kJ mol^{-1} or more negative involve charge sharing or transfer from the inhibitor molecules to the metal surface to form a coordinate type bond. This corresponds to chemisorptions [78-81]. In our study the physisorption mode is likely to predominate due to the obtained value of ΔG°_{ads}(-22.80 kJ mol^{-1}).

3.3. Quantum-chemical calculations

3.3.1. Global reactivity descriptors

Quantum chemical calculations have been widely used to study the reactivity of organic compounds[82,83]. The inhibition potential of camphor has been elucidated using quantum chemical calculations based on density functional theory (DFT). Hence, we have investigated the relationship between the molecular structure, the

electronic structure and the inhibition efficiency of the studied molecule. Full geometry optimization (Figure 13) with no constraints of camphor was performed using DFT based on the Becke's three parameter exchange functional and the Lee–Yang–Parr nonlocal correlation functional (B3LYP) ,as well as the 6-31G* orbital basis set for all atoms as implemented in the Gaussian 09 program [53]. This approach has been proved to be a very powerful tool for studying corrosion inhibition mechanism [84-86] consistent reaction field) was used to perform the calculation in aqueous SCRF method [87] solution.

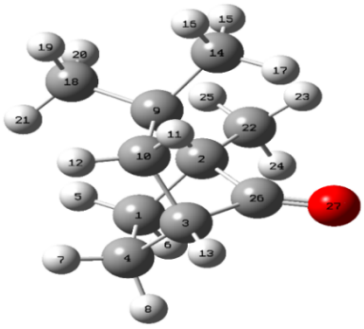

Figure 13: Optimized structure of camphor as calculated at the B3LYP/6-31G* level

The quantum chemical parameters of the camphor molecule such as total energy (TE), E_{HOMO} (highest occupied molecular orbital energy), E_{LUMO} (lowest unoccupied molecular orbital energy), the energy gap (ΔEg), electron affinity (EA), ionization potential (IP), the absolute electronegativity (χ), the hardness (η), the Global chemical softness (S), dipole moment (μ) and the fraction of electrons (ΔN) in aqueous solution, were calculated and gathered in Table 6.

Table 6: Calculated quantum chemical parameters of camphor in aqueous solution

Quantum parameters	Camphor
TE (a, u)	-465.93
E_{HOMO}(ev)	-6.170
E_{LUMO}(ev)	-0.190
ΔEg (ev)	5.980
μ (debye)	2.800
S	0.333
IP (ev)	6.170
χ(ev)	3.180
EA (ev)	0.190
η (eV)	3.000
ΔN	0.639

The frontier molecular orbital HOMO and LUMO of a given chemical compound are very important in defining its reactivity. Survey of literature[88–90] shows that the adsorption of the inhibitor on the metal surface can occur on the basis of donor–acceptor interactions between the π-electrons of the heteroatom (-O-) in a compound and the vacant d-orbital of the metal surface atoms [91].The Table 6 shows the TE, E_{HOMO} and E_{LUMO}. A high value of E_{HOMO} corresponds to a tendency of the molecule to donate electrons to appropriate acceptor molecules of low LUMO energy [92]. The inhibitor does not only donate electrons to the unoccupied d-orbital of the metal ion but can also accept electrons from the d-orbital of the metal leading to the formation **of a feed-back bond**. The values of theoretical parameters such as E_{LUMO} = -0,19eV and E_{HOMO} =-6,17eV presented in Table 6 are in good correlation with the distribution of HOMO and LUMO orbitals. The highest value of the E_{HOMO} of the studied compound indicates the better inhibition efficiency. Therefore, the tendency for the formation of a feed-back bond would depend on the values of E_{LUMO}. The lower value of the E_{LUMO} leads to suggestion that the acceptance of electrons from the d-orbital of the metal is easier. It is well known that larger values of the energy gap ΔE_g, will lead to low reactivity with chemical species [93, 94]. Conversely,

lower values of the ΔEg will correspond to good inhibition efficiency, because the energy required to remove an electron from the lowest occupied orbital will be low. From Table 6, the calculation indicates that the small value of ΔE_g(5,98 eV) which means the highest reactivity and accordingly the highest inhibition efficiency. This agrees well with experimental observations. The inhibition effect of a given compound is usually ascribed to the adsorption of the molecule on the metal surface. There can be physical adsorption (physisorption) and chemical adsorption (chemisorption) depending on the adsorption strength. When chemisorption takes place, one of the reacting species acts as an electron pair donor and the other one act as an electron pair acceptor. The ground state geometry of the inhibitor as well as the nature of its frontier molecular orbitals, namely the HOMO and LUMO is involved in the activity properties of the inhibitor. In this study, the HOMO and LUMO are delocalised over the entire molecule of camphor. We have recalculated the proprieties of the molecule in aqueous solution. We found that the shapes of the HOMO and LUMO do not change compared to the gas phase. Hence, the shape of the HOMO and LUMO is independent of the environment of the molecular system. In Figure 14, we present the frontier molecule orbital density distributions of the studied compound. It can be seen that the electronic densities of the HOMO and LUMO are delocalized almost over the entire molecule. These atoms are the favourite sites for adsorption [95,96].

Figure 14: Schematic representation of HOMO and LUMO molecular orbital of camphor

Another method to correlate inhibition efficiencies with parameters of molecular structure is to calculate the fraction of electrons transferred from the inhibitor to the metal surface. According to Koopman's theorem [93], E_{HOMO} and E_{LUMO} of the inhibitor molecule are related to the ionization potential (IP) and the electron affinity (EA), respectively. The ionization potential and the electron affinity are defined as IP = - E_{HOMO} and EA = - E_{LUMO}, respectively. Then the absolute electronegativity (χ) and the global hardness (η) of the inhibitor molecule are approximated as follows [97,98]:

$$\chi = \frac{\mathrm{IP} + \mathrm{EA}}{2} \qquad (16)$$

$$\eta = \frac{\mathrm{IP} - \mathrm{EA}}{2} \qquad (17)$$

Hardness (η) and softness (S) are global chemical descriptors measuring the molecular stability and reactivity. There is related by:

$$\mathrm{S} = \frac{1}{\eta} \qquad (18)$$

The chemical hardness is the resistance against the deformation or polarization of the electron cloud of the atoms, ions or molecules under small perturbations in a chemical reaction. A hard molecule has a large energy gap and a soft molecule has a small energy gap [95]. In our study, the smallest energy gap is encountered for camphor in aqueous solution. There, we have found the highest value of softness (S= 0,334eV) and the lowest value of hardness (η =3.00 eV). Normally, the inhibitor with the lowest value of global hardness (respectively, the highest value of global softness) is expected to have the highest inhibition efficiency [96]. In fact, soft molecules are more reactive than hard ones because they could easily offer electrons to an acceptor. Thus, for the simplest transfer of electron, adsorption could occur at the part of the molecule where softness(S), which is a local property, has a highest value [97]. Hence, in the present work, our calculations confirm the highest inhibition efficiency of the studied compound. Another quantity, called the fraction of electrons (ΔN) transferred can be evaluated by Pearson electronegativity scale:

$$\Delta\mathrm{N} = \frac{\emptyset - \eta_{\mathrm{inh}}}{2(\eta_{\mathrm{Fe}} + \eta_{\mathrm{inh}})} \qquad (19)$$

Where Ø is the work function of the iron surface with the value of 4.06 eV for Fe (1 1 0) [99,100], χ_{inh} is the absolute electronegativity associated to the inhibitor molecule, $\eta_{Fe} = 0$ and η_{inh} are the absolute hardness of metal and the inhibitor molecule, respectively. It has also reported that the ΔN value measures the ability of a chemical compound to transfer its electrons to metal if $\Delta N > 0$ and vice versa if $\Delta N < 0$ [101,102]. In this study, the positive value of ΔN = 0,639 presented in Table 6, suggest the high capability of camphor to donates electrons to the carbon steel surface. In general, the atomic charges of the inhibitor and the dipole moment (μ) in particular are important electronic parameters that increase the adsorption between a chemical compound and a metal surface [88]. In our study, the value of the dipole moment is 2,803 Debye in aqueous solution. This means a better inhibition efficiency.

3.3.2. *Fukui Functions*

Fukui functions are parameters that determine the type of attack (nucleophilic, electrophilic or radical). There a may be a competition between the three types of attack. The fukui functions provide us with a measure of the change in the density with respect to a change in the number of electrons[92, 102, 103]. The Fukui functions are be defined as follows[104, 106]:

$$f_k^+ = P_k(N+1) - P_k(N) \text{(For nucleophilic attack)} \quad (20)$$

$$f_k^- = P_k(N) - P_k(N-1) \text{(For electrophilic attack)} \quad (21)$$

Where the densities of the cation $P_k(N-1)$, the neutral P_k (N), and the anion P_k (N + 1) are used. The molecule of camphor can donate electrons to the metal surface and also can accept electrons. It is important to look at the active sites responsible for giving or accepting electrons that can be derived by evaluating the Fukui functions. The calculated Fukui functions of camphor are presented in Table 7.

Table 7: Fukui functions calculated at B3LYP/6-31G*

Atoms	ρ(N)	ρ(N-1)	ρ(N+1)	f_k^{+-}	f_k^+
C 1	-0.44967	-0.46397	-0.42388	+0.0143	+0.02579
C 2	-0.15179	-0.07059	-0.12851	-0.0812	+0.02328
C 3	-0.33525	-0.28112	-0.30389	-0.05413	+0.03136
C 4	-0.45532	-0.46853	-0.42769	0.01321	+0.02763
C 9	-0.04633	-0.04229	-0.04674	-0.00404	-0.00041
C 10	-0.45805	-0.45945	-0.41819	+0.0014	+0.03986
C 14	-0.67674	-0.6993	-0.63436	+0.02256	+0.04238
C 18	-0.66815	-0.6862	-0.6331	+0.01805	+0.03505
C 22	-0.66997	-0.70536	-0.62148	+0.03539	+0.04849
C 26	+0.59663	+0.65726	+0.26747	-0.06063	-0.32916
O 27	-0.53122	-0.19371	-0.85492	-0.33751	-0.3237

Table 7 represents the effective atomic charges from the Mulliken population analysis of camphor, From this Table, the oxygen and C26 atoms in the camphor compound, have high negative charge densities, and present the highest values of f_k^- and f_k^+, respectively, implying that the most probable reactive sites for the adsorption of camphor on a carbon steel surface is located on this atom. For a finite system such as an inhibitor molecule, when the molecule is accepting electrons, one has f_k^-, the index for nucleophilic attack; when the molecule is donating electrons, one has f_k^+, the index for electrophilic attack. This observation confirms the high importance of the heteroatoms in a heterocyclic ring, on the adsorption of the organic compounds on the carbon steel surface.

3.3.3. Mulliken charge analysis

The Mulliken population analysis is an important type of calculation. It is used to investigate the electronic charges on the atoms of the molecule, Table 8 present the Mulliken charges of non-hydrogen atoms. Table 8 represents the effective atomic charges from a Mulliken population analysis of camphor in aqueous solution. From this Table, the most negative charges are located on the oxygen atom. These finding is due to the electronegativity of the oxygen atom.

Table 8: Effective atomic charges from Mulliken populations of camphor

Atomes	Mulliken Charges
1 C	-0.195629
2 C	-0.007472
3 C	-0.126703
4 C	-0.189639
9 C	+0.051432
10 C	-0.185062
14 C	-0.322118
18 C	-0.317680
22 C	-0.322818
26 C	+ 0.42073
27 O	-0.455626

The atoms carrying negative can offer electrons to the Fe atoms to form coordinate bonds. The atoms carrying positive charges can accept electrons from Fe atomic orbitals to form feed-back bonds.Thus, the optimized structure is in accordance with the fact that an excellent corrosion inhibitor can not only offer electrons to unoccupied orbital of the metal but also accepts free electrons from the metal. Therefore, it can be inferred that the oxygen atom is the possible active adsorption site. These results are in good agreement with the Fukui functions result. Besides, the atoms (C_{22}, C_{18}, C_{14}, C_{10}, C_4, C_3, C_2 and C_1) bear significant negative charges. This is due to the mesomeric effect between the cyclic ring and the=C=O function. This delocalized character of the electrons leads to a more stable form structure of camphor.

3.4. Molecular Dynamic (MD) simulation

The interaction energy (E_{int}) of inhibitor with Fe (110) surface was obtained using the following equation:

$$E_{int} = E_{total} - (E_{surface + solution} + E_{inhibitor + solution}) + E_{solution}$$

Where E_{total} is the total energy of the entire system; $E_{surface+ solution}$ is the total energy of Fe (110) surface and solution without camphor; $E_{inhibitor + solution}$ is the total energy of camphor and solution and $E_{solution}$ is the total energy of the water molecules.

The binding energy is the negative of the interaction energy and is given as: $E_{binding} = -E_{int}$

Figure 15 shows equilibrium adsorption of camphor on Fe (110) surface in the presence of 500 molecules of water. Also Table 8 presents the interaction energy (E_{int}) of the adsorption of camphor on Fe (110) surface.

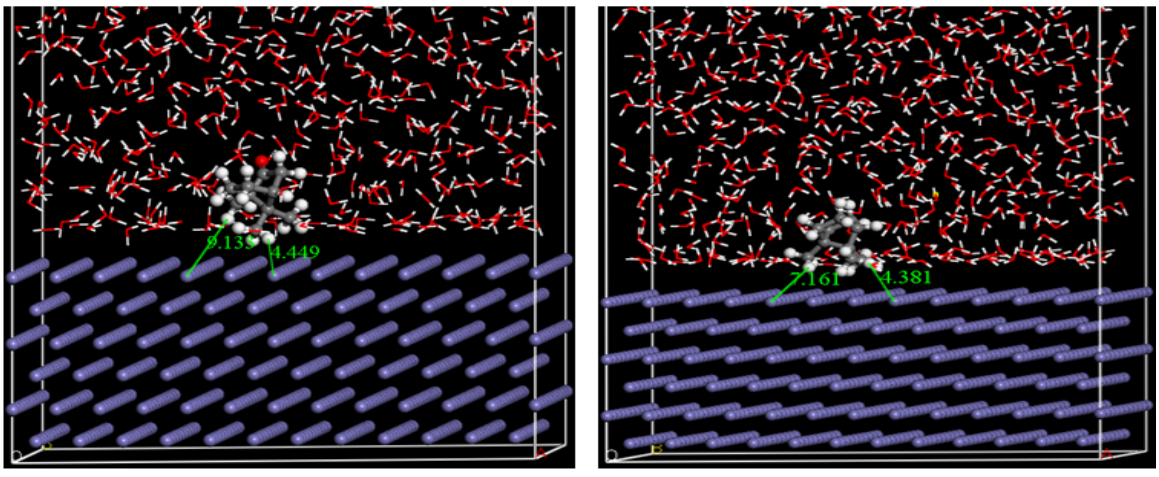

(a) (b)

Figure 15: (a) Initial configuration of camphor molecule on Fe (110) surface in the presence of 500 water molecules (Camphor was visualized by balls and sticks, and water molecule by lines) and (b) Final equilibrium configuration of the MD simulation box (adsorption behavior of camphor on the Fe (110) surface

The interaction energy is regarded as indication of the stability of adsorption system. Large negative value of interaction energy guarantees an easier adsorption of inhibitors on the iron surface and by extension higher inhibition efficiency [55]. The calculated value of E_{int} is -178.36 kcal/mol for camphor adsorbed on steel surface (table 9). Therefore, camphor is expected to binds stronger on carbon steel surface in the presence of water. This ensures effective inhibition of corrosion of carbon steel.

Table 9: Interaction energy (E_{int}) of camphor adsorption on Fe (110) surface in the presence of 500 molecules of water (kcal/mol)

E_{total}	$E_{surface+solution}$	$E_{inhibitor+solution}$	$E_{solution}$	E_{int}	$E_{binding}$
-85601.89	-85556.87	-3597.39	-3611.06	-178.36	178.36

Conclusion

It can be concluded as follows:

1. Camphor acts as good carbon steel corrosion inhibitor in hydrochloric acid.
2. PDP measurements demonstrate that the Camphor act as a mixed-type inhibitor.
3. In all tested experimental methods, the IE% increase with the rise in Camphor concentration.
4. The adsorption of the Camphor on the steel surface obeys the Langmuir adsorption isotherm. The adsorption occurs by physical interactions
5. The results obtained from PDP and EIS are in good agreement.
6. The molecular modelling including, Quantum-chemical calculations method and MD simulations support the good

References

1. I. Ahamad, R. Prasad, M.A. Quraishi, *Corros. Sci.* 52 (2010) 1472-1481.
2. A.K Singh, M.A Quraishi, *Corros. Sci.* 52 (2001) 152-160.
3. L.R Chauhan, G. Gunasekaran, *Corros. Sci*. 49 (2007) 1143-1161.
4. Y. Abboud, A. Abourriche, T. Saffaj, M. Berrada, M. Charrouf , A. Bannamara, N. Al-Himidi, H. Hannache, *Mater. Chem. Phys*. 105 (2007) 1-5.
5. F. Eghbali, M.H. Moayed, A. Davoodi, N. Ebrahimi, *Corros. Sci*. 53 (2011) 513.
6. F. Bentiss, M. Lebrini, M. Traisnel, M. Lagrenee, *J. Appl. Electrochem.* 39 (2009) 1399.
7. P.C. Okafor, M.E. Ikpi, I.E. Uwaha, E.E. Ebenso, U.J. Ekpe, S.A. Umoren, *Corros. Sci.* 50 (2008) 2310.
8. E. Khamis, *Corrosion.* 46 (1990), 476.
9. E. Stupnisek-Lisac, S. Podbrscek, *J. Appl. Electrochem*. 24 (1994) 779.
10. E. Stupnisek-Lisac, M. Metikos-Hukovic, *Br. Corros. J.* 28 (1993) 74.
11. S.L. Granese, B.M. Rosales, C. Oviedo, J.O. Zerbino, *Corros. Sci*. 33 (1992) 1439.
12. S.L. Granese, *Corrosion*. 44 (1988) 322.
13. M.A. Quraishi, H.K. Sharma, *Chem. Phys.* 78 (2002) 18.
14. M.A. Quraishi, R. Sardar, *Mater. Chem. Phys*. 78 (2002) 425.
15. M. Mihit, K. Laarej, H. Abou El Makarim, L. Bazzi, R. Salghi, B. Hammouti, *Arab. J. Chem.* 3 (2010) 55.
16. A.H. Al Hamzi, H. Zarrok, A. Zarrouk, R. Salghi, B. Hammouti, S.S. Al-Deyab, M. Bouachrine, A. Amine, Guenoun, *Int. J. Electrochem. Sci*. 8 (2013) 2586.
17. A. Zarrouk, B. Hammouti, H. Zarrok, I. Warad, M. Bouachrine, *Der Pharm. Chem.* 3 (2011) 263.
18. D. Ben Hmamou, R. Salghi, A. Zarrouk, M. Messali, H. Zarrok, M. Errami, B. Hammouti, Lh. Bazzi, A. Chakir, *Der Pharm. Chem.* 4 (2012) 1496.
19. A. Ghazoui, N. Bencaht, S.S. Al-Deyab, A. Zarrouk, B. Hammouti, M. Ramdani, M. Guenbour, *Int. J. Electrochem. Sci*. 8 (2013) 2272.
20. A. Zarrouk, H. Zarrok, R. Salghi, N. Bouroumane, B. Hammouti, S.S. Al-Deyab, R. Touzani, *Int. J. Electrochem. Sci*. 7 (2012) 10215.
21. H. Bendaha, A. Zarrouk, A. Aouniti, B. Hammouti, S. El Kadiri, R. Salghi, R. Touzani, *Phys. Chem. News*. 64 (2012) 95.
22. S. Rekkab, H. Zarrok, R. Salghi, A. Zarrouk, Lh. Bazzi, B. Hammouti, Z. Kabouche, R. Touzani, M. Zougagh, *J. Mater. Environ. Sci.* 3 (2012) 613.
23. A. Zarrouk, B. Hammouti, H. Zarrok, M. Bouachrine, K.F. Khaled, S.S. Al-Deyab, *Int. J. Electrochem. Sci*. 6 (2012) 89.
24. A. Ghazoui, R. Saddik, N. Benchat, M. Guenbour, B. Hammouti, S.S. Al-Deyab, A. Zarrouk, *Int. J. Electrochem*. *Sci.* 7 (2012) 7080.

25. H. Zarrok, K. Al Mamari, A. Zarrouk, R. Salghi, B. Hammouti, S.S. Al-Deyab, E. M. Essassi, F. Bentiss, H. Oudda, *Int. J. Electrochem. Sci*. 7 (2012) 10338.
26. H. Zarrok, A. Zarrouk, R. Salghi, Y. Ramli, B. Hammouti, M. Assouag, E.M. Essassi, H. Oudda, M. Taleb, *J. Chem. Pharm. Res*. 4 (2012) 5048.
27. A. Zarrouk, B. Hammouti, A. Dafali, F. Bentiss, *Ind. Eng. Chem. Res*. 52 (2013) 2560.
28. H. Zarrok, A. Zarrouk, R. Salghi, H. Oudda, B. Hammouti, M. Assouag, M. Taleb, M. Ebn Touhami, M. Bouachrine, S. Boukhris, *J. Chem. Pharm. Res.* 4 (2012) 5056.
29. H. Zarrok, H. Oudda, A. El Midaoui, A. Zarrouk, B. Hammouti, M. Ebn Touhami, A. Attayibat, S. Radi, R. Touzani, *Res. Chem. Intermed*. 38 (2012) 2051.
30. A. Ghazoui, A. Zarrouk, N. Bencaht, R. Salghi, M. Assouag, M. El Hezzat, A. Guenbour, B. Hammouti, *J. Chem. Pharm. Res.* 6 (2014) 704.
31. H. Zarrok, A. Zarrouk, R. Salghi, M. Ebn Touhami, H. Oudda, B. Hammouti, R. Touir, F. Bentiss, S.S. AlDeyab, *Int. J. Electrochem. Sci*. 8 (2013) 6014.
32. A. Zarrouk, H. Zarrok, R. Salghi, R. Touir, B. Hammouti, N. Benchat, L.L. Afrine Hannache, M. El Hezzat, M. Bouachrine, *J. Chem. Pharm. Res.* 5 (2013) 1482.
33. H. Zarrok, A. Zarrouk, R. Salghi, M. Assouag, B. Hammouti, H. Oudda, S. Boukhris, S.S. Al Deyab, I. Warad, *Der Pharm. Lett.* 5 (2013) 43.
34. D. Ben Hmamou, M.R. Aouad, R. Salghi, A. Zarrouk, M. Assouag, O. Benali, M. Messali, H. Zarrok, B. Hammouti, *J. Chem. Pharm. Res*. 4 (2012) 3498.
35. M. Belayachi, H. Serrar, H. Zarrok, A. El Assyry, A. Zarrouk, H. Oudda, S. Boukhris, B. Hammouti, E. Ebenso Eno, A. Geunbour, *Int. J. Electrochem. Sci.* 10 (2015) 3010.
36. H. Tayebi, H. Bourazmi, B. Himmi, A. El Assyry, Y. Ramli, A. Zarrouk, A. Geunbour, B. Hammouti, E. Ebenso Eno, *Der Pharm. Lett*. 6 (2014) 20.
37. H. Tayebi, H. Bourazmi, B. Himmi, A. El Assyry, Y. Ramli, A. Zarrouk, A. Geunbour, B. Hammouti, *Der Pharm. Chem*. 6 (2014) 220.
38. K. Boumhara, M. Tabyaoui, C. Jama, F. Bentiss, *J. Ind. Eng.Chem*. 29 (2015) 146-15.
39. N. Lotfi, F. Benhiba, N. Chahboun, H. Bourazmi, M. El Hezzat, A.H. Al Hamzi, H. Zarrok, A. Guenbour, M. Ouhssine, H. Oudda, A. Zarrouk, *Der pharm.Chem*. 7 (2015) 1-7.
40. A. El Bribri, M. Tabyaoui, B. Tabyaoui, H. El Attari, F. Bentiss, *Mat.Chem. Phys.* 141 (2013) 240-24.
41. M. Kli skic, J. Rado sevi, S. Gudi, V. Katalini, *J. Appl. Elect*. 30 (2000) 823-830.
42. I.H. Farooqi, M.A. Quraishi, P.A. Saini, *Corros. Prev. Control*. 46 (1999) 93-96.
43. R.M. Saleh, A.A. Ismail, A.A. El Hosary, *Corros. Sci.* 23 (1983) 1239-1241.
44. F. Zucchi, I.H. Omar, *Surf. Technol.* 24 (1985) 391-399.
45. P.B. Raja, M.G. Sethuraman, *Mater. Lett.* 62 (2008) 113-116.
46. R.M. Saleh, A.A. Ismail, A.A. El Hosary, Corros. *Prev. Control.* 31 (1984) 21-23. .
47. S. Garai, S. Garai, P. Jaisankar, J.K. Singh, A. Elango, *Corros. Sci.* 60 (2012) 193-204.
48. A. Bouyanzer, B. Hammouti, L. Majidi, *Mater. Lett.* 60 (2006) 2840.
49. Z. Faska, A. Belliou, M. Boukla, L. Majid, R. Fih, A. Bouyanzer, B. Hammouti, *Monatsh. Chem.* 139 (2008) 1417.
50. N. Lahhit, A. Bouyanzer, J.M. Desjobert, B. Hammouti, R. Salghi, J. Costa, C. Jama, F. Bentiss, L. Majidi, *Portug. Electrochem. Acta*. 29 (2011) 127.
51. E. Chaieb, A. Bouyanzer, B. Hammouti, M. Berrabah, *Acta. Phys. Chim. Sin.* 25 (2009) 1254.
52. J.C. Mann, J.B. Hobbs, D.V. Banthorpe, J.B. Harborne, *Natural products: their chemistry and biological significance. Longman Scientific &Technical*. (1994).
53. R. Jasinski, M. Kwiatkomska, A. Baranski, *J. Mol. Struct. Thochem. 910* (209) 80-87.
54. J. Tan, L. Guo, T. Lv, S. Zhang, *Int. J. Electrochem. Sci*. 10 (2015) 823-837.
55. I.B. Obot, Z.M. Gasem, *Corros. Sci*. 83 (2014) 359-366.
56. J.P. Zeng, J.Y. Zhang, X.D. Gong, *Theo. Chem.* 963 (2011) 110-114.
57. S. Rekkab, H. Zarrok, R. Salghi, A. Zarrouk, Lh. Bazzi, B. Hammouti, Z. Kabouche, R. Touzani, M. Zougagh, *J. Mater. Environ. Sci.* 3 (2013) 613.
58. H. Elmsellem, T. Harit, A. Aouniti, F. Malek, A. Riahi, A. Chetouani, B. Hammouti, *Prot. Meta. Phy.Chem. Sur.* 51 (2015) 873-884.
59. A. Bouyanzer, B. Hammouti, *Bull. Electr.* 52 (2004) 63-65.
60. H. Elmsellem, A. Aouniti, M. Khoutou, A. Chetouani, B. Hammouti, N. Benchat, R.Touzani, M. Elazzouzi, *J. Chem. Pharm. Res.* 6 (2014) 1216-1224.
61. A. Salhi, I. Bouyanzer, A. Hamdani, B. Chetouani, M. Hammouti, L. Znini, J. Majidi, M. Costa, *J.* El Azzouzi, *Der. Phar. Chem*. 7 (2015) 7138-147.

62. M. El Azzouzi, A. Aouniti, L. Herrag, A. Chetouani, H. Elmsellem, B. Hammouti, *J. Der. Phar. Chem.* 7 (2015) 12-24.
63. A.R. Sathiyapriya, V.S. Muralidharan, S. Subramanian. *Corrosion*. 64 (2008) 541.
64. M.S. Morad, *Corros. Sci.* 42 (2000) 1307-1326.
65. Z.B. Stoynov, B.M. Grafov, B. Savova-Stoynova, V.V. Elkin, *Elec. Imp. Nauka. Moscow*. (1991).
66. W.H. Mulder, J.H. Sluyters, *Elect. Acta*. 33 (1988) 303-310.
67. A.A. Hermas, M.S. Morad, M.H. Wahdan, *J. Appl. Elect*. 34 (2004) 95-102.
68. Z. Stoynov, *Elec. Acta*. 35 (1990) 1493-1499
69. G.J. Brug, A.L.G. Van den Eeden, M. Sluyters-Rehbach, J.H. Sluyters, *J. Elec. Chem.* 176 (1984) 275-295.
70. H. Ma, X. Cheng, G. Li, S. Chen, Z. Quan, S. Zhao, L. Niu, *Corros. Sci.* 42 (2000) 1669-1683.
71. A. Popova, M. Christov, A. Vasilev, *Corros. Sci.* 49 (2007) 3290-3302.
72. F. Bentiss, M. Lebrini, M. Lagrenée, M. Traisnel, A. Elfarouk, H. Vezin, *Elect. Acta.* 52 (2007) 6865-6872.
73. R. Kanojia, G. Singh, *Surf. Eng.* 21 (2005)180-186.
74. A. Zarrouk, B. Hammouti, T. Lakhlifi, M. Traisnel, H. Vezin, F. Bentiss, *Corros. Sci.* 90 (2015) 572-584.
75. C.H. Hsu, F. Mansfeld, *Corrosion*. 57 (2001) 747-748.
76. R. Solmaz, G. Kardas, M.C. Ulha, B. Yazıcı, M. Erbil, *Elect. Acta.* 53(2008) 5941.
77. W. Chen, H.Q. Luo, N.B. Li, *Corros. Sci*. 53 (2011) 3356.
78. S.S. Abd El-Rehim, M.A.M. Ibrahim, K.F. Khaled, *J. Appl. Electrochem.* 29 (1999) 593.
79. M. Ehteshamzadeha, A.H. Jafari, E. Naderia, M.G. Hosseini, *Mater. Chem. Phys.* 113 (2009) 986-993.
80. A.K. Singh, M.A. Quraishi, *Corros. Sci.* 53 (2011) 1288-1297.
81. M.J. Bahrami, S.M.A. Hosseini, P. Pilvar, *Corros. Sci.* 52 (2010) 2793-2803.
82. M. Behpour, S.M. Ghoreishi, N. Mohammadi, N. Soltani, S. Salavati-Niasari , *Corros. Sci.* 52 (2010) 4046-4057.
83. R.N. Singh, A. Kumar, R.K. Tiwari, P. Rawat, *Spectrochim. Acta. A. Mol. Biomol. Spectrosc*. 112 (2013) 182-190.
84. H. Jafari, I. Danaee, H. Eskandari, M. Rashvand Avei, *J. Mater. Sci. Technol*. 30 (2014) 239-252.
85. L.M. Rodríguez-Valdez, W. Villamisar, M. Casales, J.G. González-Rodriguez, A. Martínez-Villafañe, L. Martinez, D. Glossman-Mitnik, *Corros. Sci.* 48 (2006) 4053-4064.
86. D. Daoud, T. Douadi, H. Hamani, S. Chafaa, M. Al-Noaimi, *Corros. Sci.* 94 (2015) 21-37.
87. I.B. Obot, D.D. Macdonald, Z.M. Gasem, *Corros. Sci.* 99 (2015) 1-30.
88. P. Gedeck, S. Schneider, *Photochem.photobiol*. 121 (1999) 7-15.
89. N.A. Wazzan, *J. Ind. Eng. Chem.* 26 (2015) 291-308.
90. I. Danaee, O. Ghasemi, G.R. Rashed, M. Rashvand Avei, M.H. Maddahy, *J. Mol. Struct.* 1035 (2013) 247-259.
91. K. Ramya, R. Mohan, K. Anupama, A. Joseph, *Mater. Chem. Phys.* 149 (2015) 632-647.
92. H. Lgaz, R. Salghi, S. Jodeh, B. Hammouti, *J. Mol. Liq.* 225 (2017) 271-280.
93. L. Feng, H. Yang, F. Wang, *Electrochimica Acta*. 58 (2011) 427-436.
94. A. Khadiri, R. Saddik, K. Bekkouche, A. Aouniti, B. Hammouti, N. Benchat, M. Bouachrine, R. Solmaz, *Taiwan Inst J. Chem. Eng.* 58 (2016) 552-564.
95. F. Kandemirli, S. Sagdinc, *Corros. Sci*. 49 (2007) 2118-2130.
96. L. Guo, X. Ren, Y. Zhou, S. Xu, Y. Gong, S. Zhang, *Arab. J. Chem*.
97. N.O. Eddy, H. Momoh-Yahaya, E.E. Oguzie, J. *Adv. Res*. 6 (2015) 203-217.
98. R.G. Pearson, *Inorg. Chem*. 27 (1988) 734-740.
99. V. Sastri, J. Perumareddi, *Corrosion*. 53 (1997) 617-622.
100. I. Lukovits, E. Kalman, F. Zucchi, *Corrosion.* 57 (2001) 3-8.
101. R.G. Pearson, *Inorg. Chem*. 27 (1988) 734-740.
102. A. Kokalj, *Elect. Acta.* 56 (2010) 745-755.
103. N. Kovačević, A. Kokalj, *Corros. Sci*. 53 (2011) 909-921.
104. Z. El Adnani, M. Mcharfi, M. Sfaira, M. Benzakour, A.T. Benjelloun, M. Ebn Touhami, *Corros. Sci.* 68 (2013) 223-230.
105. H. Jafari, K. Sayin, *Taiwan Inst J., Chem. Eng.* 56 (2015) 181-190.
106. J. Saranya, P. Sounthari, K. Parameswari, S. Chitra, *Measuremen*t. 77(2016) 175-186.

(2018); http://www.jmaterenvironsci.com